

Structural health monitoring of buckling composite structures using acoustic emission

C. A. Featherston¹, M. Eaton¹, R. Pullin¹, K. M. Holford¹

keywords: Acoustic Emission, buckling, composites, structural health monitoring.

Introduction

During recent years there has been continued pressure in the aerospace industry to minimize structural weight and hence fuel consumption, leading to cost and emissions reductions. This has resulted in an increase in the use of composite materials due to their high specific strength and stiffness. These are incorporated into a series of thin stiffened shells thereby optimizing performance for a given structural mass. These shells however are subject to failure by buckling under combinations of compression, shear and in-plane bending. Buckling loads can be substantially compromised by the presence of damage (up to 30% in the case of delamination (Abrate (1994))). Composite structures are extremely susceptible to such damage which can include matrix cracking and fibre failure in addition to delamination. This can be caused by impact (i.e. dropped tools, collisions, stone chips etc) or due to manufacturing defects. One of the greatest problems with the use of composites is that this damage may not be detected visually. Techniques are therefore needed to detect unseen damage, preferably in situ, by incorporation into a structural health monitoring system (SHM) which can identify and locate damage providing information on type and severity such that appropriate action can be taken in a timely fashion to avoid structural failure. One such method is acoustic emission, which detects elastic waves emitted during the development of damage when a structure is loaded. In addition to its ability to monitor a structure in real-time, this technique has the added advantage of being passive (no input signal required), reducing the power requirements for an SHM system based on this technique substantially. This paper looks at the feasibility of such a system by detecting, characterising and locating damage occurring during the buckling and postbuckling of a panel. Specific emphasis is placed on meeting the challenges of damage identification and location in an orthotropic material.

Coupon Testing

In order to provide data to enable source characterisation in the full size panel a series of coupon tests were first performed. These included both tensile and

¹Cardiff School of Engineering, Cardiff University, Queen's Buildings, The Parade, Cardiff, CF24 3AA, UK. Tel: +44 (0) 2920875328, Fax: +44 (0) 2920874939, Email: FeatherstonCA@cardiff.ac.uk

compressive tests, designed to initiate different modes of failure which could be examined alongside the corresponding AE data. The results of the compressive tests will be presented here since they are most representative of the failure modes found during the later buckling tests.

Experimental set-up. A series of six specimens of width 30mm and length 200mm were tested. These were manufactured from ACG's HTM45/HS-135-34% RW uni-directional carbon fibre/epoxy pre-preg laid up to give three specimens with a stacking sequence of $((0,90)_4)_s$ and three with $((\pm 45)_4)_s$. Specimens were cured in a hot press at 6 bar and 175°C for 120 minutes and cut using a water cooled, diamond tipped cutting wheel. They were mounted in turn in the test cage illustrated in Figure 1 which reduced the unsupported length of each specimen to 170mm. The specimens were monitored using two Physical Acoustics Ltd PAL WD AE sensors (a wideband sensor with a good level of sensitivity across a range of frequencies) placed at 1/4 of the length, or 42.5mm from the supports, which coincides with the two inflection points and hence ensured the sensors had maximum contact with the deformed specimen. The specimens were loaded to failure at $0.5\text{mm}\cdot\text{min}^{-1}$ and $1\text{mm}\cdot\text{min}^{-1}$ for the (0,90) and (± 45) lay-ups respectively. Data was recorded throughout the test using a PAL PCI-2 system. In addition to acoustic emission monitoring, full-field displacement and strain measurements were taken throughout the test using a LIMESS Digital Image Correlation (DIC) optical system, capable of providing full field displacement, strain and curvature data for the specimen.



Figure 1: Loading cage for buckling specimen

Results and discussion After initial buckling, (Figure 2) the $((\pm 45)_4)_s$ specimens (most representative of the area of interest in the full-size panel) fail by delamination both in the surface plies adjacent to the supports on the compressive side of the specimen and in the mid-ply also adjacent to the supports (Figure 3). Details of the curvature (indicative of the degree of inter-laminar shear and seen to be greatest adjacent to the supports (Figure 2)) were recorded at the point of delamination using data obtained from the DIC system. Values of maximum curvature at the point of delamination were found to be consistent for each of the two lay-ups demonstrating the repeatability of the test. (Data for a $((\pm 45)_4)_s$ lay-up is presented in Table 1).

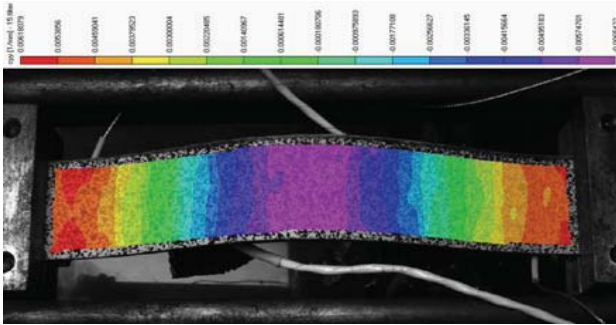


Figure 2: Curvature contour for buckling specimen

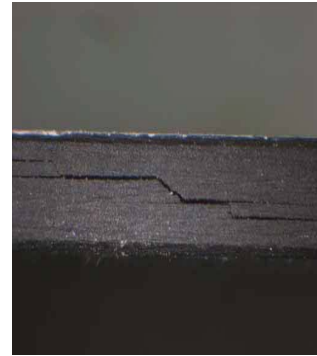
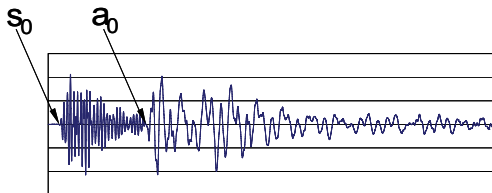


Figure 3: Delamination failure

Table 1: Curvature at delamination initiation for beam buckling specimens 4-6 ((±45)₄)

Specimen	1	2	3
Curvature (mm ⁻¹)	0.00648	0.00618	0.00650

Amplitude ratios for AE signals occurring at the time of delamination were also calculated. AE signals propagate as plate modes in thin plate-like structures with an in-plane symmetric mode s_0 and an out-of-plane anti-symmetric mode a_0 which are identified for a typical AE signal in Figure 4. In-plane sources of damage (eg. matrix cracking) produce signals with larger amplitude s_0 modes. Out-of-plane sources (e.g. delamination) produce signals with a larger amplitude a_0 mode. The amplitude ratio defined below has been identified by previous authors working with artificial signals (Surgeon, M. and Wevers (1999), Prosser (1996)) as providing a potential signal discriminator, allowing specific signals to be associated with an appropriate failure mode.



$$\text{Amplitude ratio} = \frac{s_0}{a_0}$$

Figure 4: Signal amplitude ratio

The amplitude ratios of signals from the delaminations observed in the ±45° beam buckling specimens were observed to be mostly below 1 as indicated in Figure 5, in contrast to those produced by in-plane sources during the tensile tests (which failed by matrix cracking) which generally produced signals with ratios between 0.5 and 5.

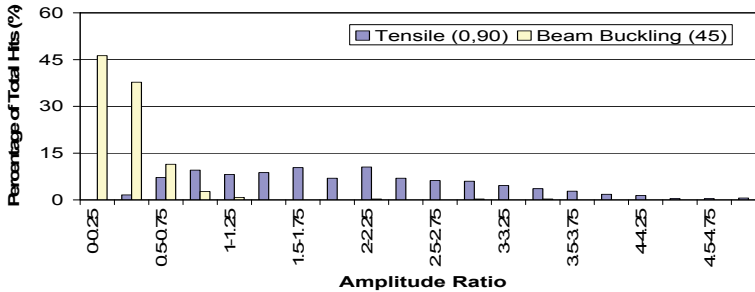


Figure 5: Amplitude ratios for signals generated by coupon tests

Large Scale Testing

A series of large scale buckling tests were then performed in order to demonstrate the ability of AE testing to identify and locate damage in a more realistically sized structure.

Test set-up A total of 8 specimens with width 410mm and height 380mm were manufactured with a $(0,90)_{4S}$ lay-up. The specimens were manufactured from ACG's HTM45/HS-135-34%RW and cured at 6 bar and 175°C for 120 minutes in an autoclave. One of the specimens was left undamaged, one had a single 200mm diameter PTFE disc embedded 2 plies from the surface at its centre, three had a 100mm diameter PTFE disc embedded 2 plies from the surface at their centres and the remaining three had a 50mm diameter PTFE disc embedded 2 plies from the surface at their centres. A speckle pattern was applied to one side of each specimen to enable the DIC system to be used. The impacted specimens were speckled on their non-impacted side and the artificially delaminated specimens were speckled on the surface closest to the PTFE insert. Each panel was tested using the buckling rig shown in Figure 6, which provides simple support to all four edges of the specimens whilst facilitating the application of a uni-axial in-plane compressive load. The vertical (unloaded) specimen edges are held between opposed knife edges (reducing the effective width to 380mm) whilst the loaded edges are supported by a series of bearings with the top edge free to move in a vertical direction. This creates a simply supported buckling area of 380mm×380mm. Specimens were loaded to failure at a rate of 0.25mm.min⁻¹ under displacement control using a Howden universal test machine.

The specimens were instrumented with eight sensors, four PAL WD sensors arranged in a 280mm×280mm square array and four PAL Nano30 sensors (a resonant sensor with a peak frequency response at approximately 300kHz, but a relatively broad frequency response for a resonant sensor) arranged 260mm apart in a diamond shaped array. Monitoring was conducted with a PAL PCI-2 system. Source location was achieved using the DeltaT method developed at Cardiff. Application

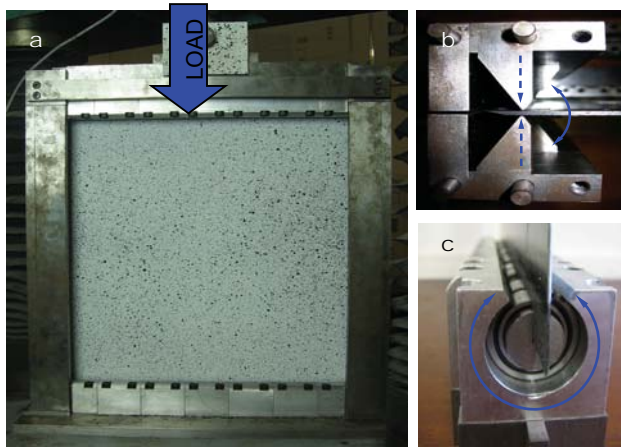


Figure 6: Test Rig a) Assembled b) Knife edges c) Roller supports

of this technique involves drawing a grid (in this case a $350\text{mm} \times 350\text{mm}$ grid with a resolution of 50mm) onto the specimen. Before each test, the response from each set of sensors (in terms of differences in signal arrival times) to a series of artificial AE sources created by breaking a pencil lead (ASTM(1994)) at each point on the grid is mapped. Hits recorded during a test can then be located based on interpreting sensor response (Baxter (2007)). Images for DIC were captured at a rate of 0.5Hz until failure and the test load at the point of capture was recorded with each image.

Results and discussion As with the coupon tests, specimens fail following initial buckling, due to delaminations propagating from the corners of the panels (demonstrated by the C-scan presented in Figure 8), where curvature (Figure 7) is highest.

Due to the loss of DIC data around the edge of the specimen (where it is obscured from the cameras used to monitor the test by the test rig) it is not possible to determine values for curvature in the corners of the specimen where the damage is initiated directly. Values have therefore been obtained by extrapolating data measured further into the specimen (Figure 9). These are presented for a range of the specimens tested in Table 2. Values are calculated at angles of $\pm 45^\circ$ to the fibres corresponding to the curvature measurements presented for the coupon specimens. Although not identical to those values found for the coupon tests (possibly due to the fact that the large-scale tests use a doubly curved panel) they are of the same order of magnitude suggesting a similar level of interlaminar shear strain as that causing delamination in the smaller specimens.

AE signal location data obtained using the Delta-T method and presented in

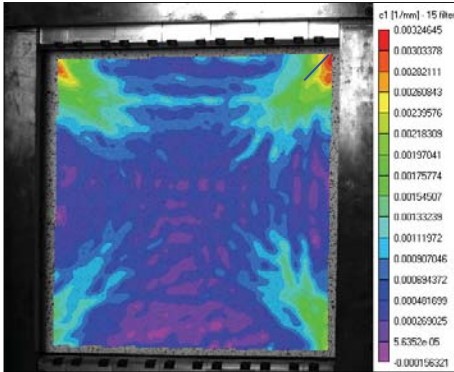


Figure 7: Principal curvature of specimen 1 at the time of arrival of the first delamination signals

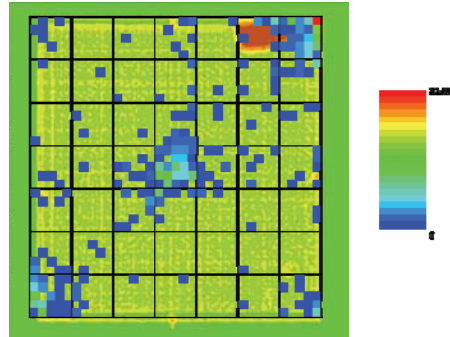


Figure 8: Location of AE hits compared with damage

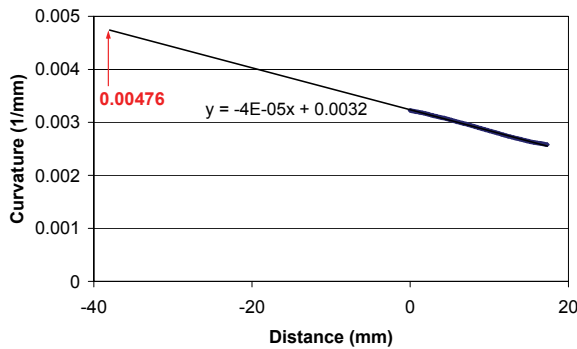


Figure 9: Curvature extrapolation

Table 2: Extrapolated curvature values at the time of arrival of the first delamination signals

Specimen	1	2	3	4	5	6	7	8
Curvature (mm ⁻¹)	0.0048	0.0040	0.0050	0.0039	0.0045	0.0050	0.0051	0.0057

Figure 8 shows excellent correlation with the damage illustrated using C-scanning. Furthermore, signals indicate possible damage initiation in the upper left and lower right hand corners of the specimen currently too small to be detected using C-scans, illustrating increased sensitivity.

Amplitude ratios for signals located in areas of delamination damage are mostly below 1 as was the case for the coupon bucking tests demonstrating the ability of AE to differentiate this type of damage.

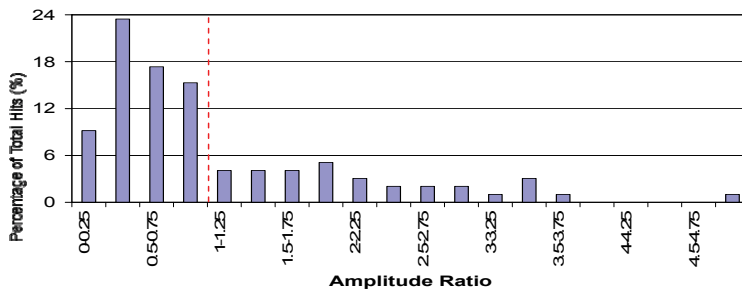


Figure 10: Amplitude ratios for signals generated by large-scale tests

Conclusions

AE techniques have been shown to successfully detect and identify delamination failure in a composite plate subject to uniaxial compression. Using the Delta-T method developed at Cardiff University this damage has been accurately located and found to occur in areas of high curvature near to the corners of the plate. The results of this work indicate the potential for using AE methods in building a suitable SHM system for aerospace structures.

References

1. Abrate, S. (1994) Impact on Laminated Composite Materials, *Applied Mechanics Review*, Vol.47(11), pp. 517-544.
2. ASTM (1994) A Standard Guide for Determining the Reproducibility of Acoustic Emission Sensor Response, *American Society for Testing and Materials*, E976.
3. Baxter, M.G. (2007) Damage Assessment by Acoustic Emission (AE) During Landing Gear Fatigue Testing. Cardiff University.
4. Surgeon, M. and Wevers, M. (1999) Modal analysis of acoustic emission signals from CFRP laminates. *NDT & E International*, 32, pp. 311-322.
5. Prosser, W.H. (1996) Advanced AE Techniques in Composite Materials Research. *Journal of Acoustic Emission*, 14, pp. 1-11.

